

Health monitoring of a new hysteretic damper subjected to earthquakes on a shaking table

L. Romo^{1a}, A. Benavent-Climent^{2b}, L. Morillas^{3c}, D. Escolano^{3d} and A. Gallego^{*1}

¹*Department of Applied Physics University of Granada, Spain*

²*Department of Mechanics of Structures and Industrial Constructions Polytechnic University of Madrid, Spain*

³*Department of Structural Mechanics University of Granada, Spain*

(Received November 11, 2013, Revised May 10, 2014, Accepted May 20, 2014)

Abstract. This paper presents the experimental results obtained by applying frequency-domain structural health monitoring techniques to assess the damage suffered on a special type of damper called Web Plastifying Damper (WPD). The WPD is a hysteretic type energy dissipator recently developed for the passive control of structures subjected to earthquakes. It consists of several I-section steel segments connected in parallel. The energy is dissipated through plastic deformations of the web of the I-sections, which constitute the dissipative parts of the damper. WPDs were subjected to successive histories of dynamically-imposed cyclic deformations of increasing magnitude with the shaking table of the University of Granada. To assess the damage to the web of the I-section steel segments after each history of loading, a new damage index called Area Index of Damage (AID) was obtained from simple vibration tests. The vibration signals were acquired by means of piezoelectric sensors attached on the I-sections, and non-parametric statistical methods were applied to calculate AID in terms of changes in frequency response functions. The damage index AID was correlated with another energy-based damage index -ID- which past research has proven to accurately characterize the level of mechanical damage. The ID is rooted in the decomposition of the load-displacement curve experienced by the damper into the so-called skeleton and Bauschinger parts. ID predicts the level of damage and the proximity to failure of the damper accurately, but it requires costly instrumentation. The experiments reported in this paper demonstrate a good correlation between AID and ID in a realistic seismic loading scenario consisting of dynamically applied arbitrary cyclic loads. Based on this correlation, it is possible to estimate ID indirectly from the AID, which calls for much simpler and less expensive instrumentation.

Keywords: seismic-resistant structures; hysteretic dampers; piezoceramic sensors; structural health monitoring; non-parametrical methods; seismic loads; damage index

1. Introduction

*Corresponding author, Professor, E-mail: antolino@ugr.es

^aPh.D., E-mail: lyrome@ugr.es

^bProfessor, E-mail: amadeo.benavent@upm.es

^cPh.D., E-mail: lmorillas@ugr.es

^dPh.D., E-mail: descolano@ugr.es

Passive control is nowadays widely recognized as an innovative technology for protecting buildings against earthquakes and preventing or drastically reducing plastic deformation (damage) to the structural elements of the main frame. A typical building structure with passive control systems consists of a moment resisting frame (referred to as “main frame” hereafter) and a series of special energy dissipating devices (EDDs), also called dampers, which connect every two consecutive floors. The principal role of the main frame is to sustain the gravity loads while the frame deforms laterally within the elastic range, due to the ground motion. In turn, the role of the dampers is to dissipate most of the energy input by the earthquake (Benavent-Climent *et al.* 2011a). The EDDs provide for greater lateral stiffness and lower yield displacement than the main structure, meaning that they concentrate the damage caused by an earthquake while the main frame remains basically elastic (undamaged). After the earthquake, the damage is limited to the EDDs, while the main frame remains undamaged (i.e., basically elastic). After several earthquakes, if the health of the EDDs is not satisfactory they may be replaced, making the building ready to sustain future ground motions. In this sense, the EDDs function like “fuses” that protect the main structure against damage from earthquakes.

Different types of EDDs (Christopoulos and Filiatrault 2006, Symans *et al.* 2008) have been developed and used so far for the passive control of structures (viscous dampers, friction dampers, viscoelastic dampers, etc.). Among them, the so-called hysteretic damper is one of the most widely used due to its favorable balance between cost and performance, and the fact that it is maintenance-free. In hysteretic dampers, the source of energy dissipation is the plastic deformation of metals (commonly steel). Several types of hysteretic dampers proposed in the literature can be installed in a frame like conventional brace elements (Black *et al.* 2004, Gray *et al.* 2010, Palermo *et al.* 2014). Yet because plastic deformations in the material involve damage, evaluating the health of the hysteretic damper after a seismic event is a matter of great significance. Indeed, monitoring the response of buildings to earthquakes is one of the most complex issues in structural engineering (Housner *et al.* 1997, Rotondo and Barbat 2004), and it is attracting increasing attention in the academic world and in the industry.

Relatively low level and frequent ground motions contribute most to damage and financial loss, while high level and rare ground motions contribute most to collapse (Goulet *et al.* 2007). Evaluating the level of damage sustained by the EDDs and whether they need to be replaced or not must be a simple and inexpensive procedure, though robust, as low level ground motions can take place several times during the life of the building. The decision as to whether it is necessary to replace the EDDs has substantial economic implications which include costs associated with the interruption of the activities of a building.

Researchers of the University of Granada have been working on the development of new EDDs suited to the demands of moderate or high seismicity regions, with a relatively low cost that makes them amenable for massive use in both new and existing structures. One recently developed damper is a hysteretic type EDD known as the Web Plastifying Damper, or WPD (Benavent-Climent *et al.* 2011a). Fig. 1 offers a schematic of this type of damper and its typical location as a conventional brace element on a building frame structure.

The WPD, based on the properties of deformation and hysteresis of steel, basically consists of several short segments of double-T structural shapes (I or H-profiles, hereafter referred to as I-sections) that are assembled on two auxiliary bars also made of steel. The I-sections are the dissipative part of the EDD, while the bars work as auxiliary elements that connect the I-section steel segments with the main frame. Fig. 2 shows a scheme of a WPD damper.

Energy dissipation on the EDD occurs when the web of the I-section undergoes out-of-plane

plastic deformation under imposed relative displacements δ between the flanges as shown in Fig. 3; when this occurs, its initial height h shortens to h' . In designing the assemblage of I-sections with auxiliary bars, this shortening must be accounted for in order to avoid spurious axial forces on the web.

The auxiliary bars are designed so that they remain elastic while the I-sections undergo plastic deformations. In addition, the auxiliary bars must have an axial stiffness that is much greater than the lateral stiffness $k=Q/\delta$ of the I-sections, where Q is the shear force acting in a single I-section

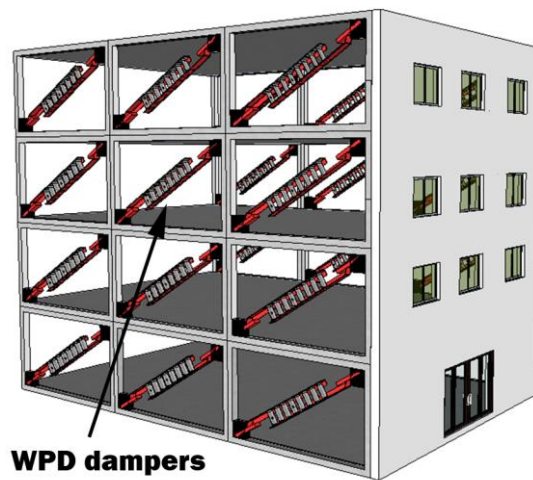


Fig. 1 Passive control systems in a building structure

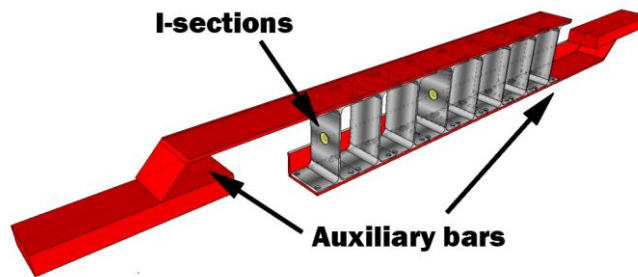


Fig. 2 Scheme of the WPD

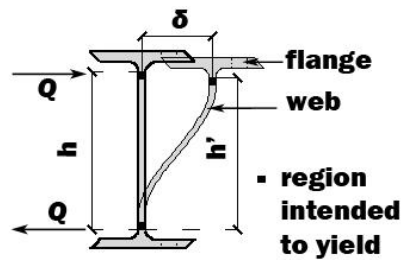


Fig. 3 Deformation of an I-section steel segment of a WPD

steel segment. Since the WPD consists of n identical I-section steel segments working in parallel, the lateral relative displacement δ between the flanges of each I-section coincides approximately with the axial deformation of the WPD, and the total axial force N opposed by the WPD to attain a given displacement δ is simply $N=nQ$.

To maintain the low cost of the WPD while also ensuring the possibility that its health be checked after a seismic event, it is necessary to develop an inexpensive measurement system providing experimental data on the condition of the EDD, as well as a robust procedure to process these data and determine the level of damage. Previous research (Benavent-Climent *et al.* 2007) has shown that the level of mechanical damage and the proximity to failure of a hysteretic type EDD subjected to arbitrarily applied cyclic loading can be accurately predicted if the history of force N and displacement δ applied to the EDD is known. The prediction consists basically of decomposing the N - δ curve into the so-called skeleton part and Bauschinger part, then calculating a damage index ID from the plastic strain energy dissipated in each part. However, measuring the force N and the displacement δ on the EDDs during an earthquake implies cumbersome and expensive instrumentation (load cells, displacement transducers, data acquisition system, etc.) that would have to be permanently installed in the building and ready for use.

Recent research (Konstantinidis *et al.* 2012) relies on computing real-time damper forces for health monitoring but this approach may not be feasible in this application. We propose that the building is inspected only after a seismic event. An alternative technique was recently put forth by the authors (Benavent-Climent *et al.* 2014, Gallego *et al.* 2012), consisting in simple vibration tests conducted by means of piezoelectric sensors directly attached to the web of the I-section, the obtained signals then being processed to calculate a damage index known as “Area Index of Damage” (AID). The AID is very well correlated with the ID, but unlike the latter index it does not require measurement during the earthquake. Vibration tests to assess the health of the EDDs are only needed after an earthquake. Furthermore, the required instrumentation is much simpler and there is no need to keep it in the building. Previous research (Benavent-Climent *et al.* 2014) on defining the experimental set-up and the numerical procedure to estimate the damage index AID was developed on the basis of static cyclic tests. Yet because earthquakes are dynamic in nature, both the experimental set-up and the data post-processing must be validated and improved under arbitrary dynamic loading. This constitutes the main objective of the present study.

In this investigation a 2/5 scale reinforced concrete frame equipped with WPDs was built and subjected to two types of tests. The first type of tests consisted in several seismic simulations conducted with a shaking table, which imposed forced axial deformations and induced several levels of damage on the WPD. The second type of tests were conducted before and after each seismic simulation and consisted on exciting (vibration tests) the web of several I-sections of the WPDs through piezoelectric ceramic actuators while the shaking table was stopped. This paper is focused on the second type of tests, which purpose was to quantify the level of damage induced on the web of the I-sections of the dampers. Accordingly, a brief description of the first type of tests is presented in sub-section 2.1, while detailed information on the second type of tests is provided in sub-section 2.2.

Forced vibrations induced by the piezoelectric ceramic actuators are very low and occur at audible frequencies, that are much higher than the fundamental frequency of the structure. As a result, the response of the web of the I-sections under the second type of tests is linear and frequency-domain methods can be applied to the processing of recorded vibration signals. Kampas (2012), Makris (2013) reported that the vibration period of bilinear systems exhibits scattering as the frequency content of the excitation widens and the acceleration response fluctuates. This is

avoided by analyzing frequencies away from the vibration period in this paper. The vibration signals recorded during the second type of tests were suitably processed to produce a quantitative assessment of the level of damage on each I-section, expressed through the AID index proposed in previous works (Benavent-Climent *et al.* 2014, Gallego *et al.* 2012). The AID was compared to the alternative mechanical damage index ID calculated from the axial load-displacement N - δ hysteretic curve of the WPD. The indexes AID and ID are found to be very well correlated by a practically linear relationship. This finding indicates that: (i) the processing technique applied for the AID damage index proposed previously based on static tests is also robust and valid for evaluating the level of damage under realistic dynamic loading as imposed by earthquakes; and (ii) the instrumentation of the I-sections used for conducting the vibration tests (i.e., piezoelectric sensors attached to the web of the I-section) is also adequate in the more demanding scenario of dynamic loads applied at higher rates than static loads.

2. Description of the experiments

2.1 Seismic simulations consisting in dynamic shaking table tests

The seismic simulations briefly described next constitute part of a much more extensive experimental campaign of dynamic shaking table tests aimed to investigate the seismic behavior of frame structures with WPDs as opposed to conventional frames without dampers. In this experimental campaign, first, a prototype structure consisting of a three-story 3×3 bay RC frame with brace-type hysteretic dampers was designed. The main frame was designed to sustain only gravitational forces. The hysteretic dampers were designed to sustain the seismic forces by applying an energy-based procedure (Benavent-Climent 2011b). This procedure provides the lateral strength and stiffness that must be supplied by the dampers for a given drift of the story and for a given design peak ground acceleration. Once the required strength and stiffness of the dampers is obtained, the dimensions of the I-section steel segments that form the WPD are determined by using design formulae (Benavent-Climent *et al.* 2011a) that depend on the yield stress and Young's modulus of the steel used, the total number of I-section segments that constitute the WPD, the length of each I-section, and the thickness and height of the web of the I-section. The seismic design assumed that the prototype structure is located in soft soil at Granada (Spain), where the design peak ground acceleration is 0.31 g (here g is the gravity acceleration).

From the prototype, a partial structural model was separated by cutting through points of nominal zero bending moment under lateral loads. From this partial structural model, the test structure was defined by applying scale factors of 2/5, 1, and 1 for length, acceleration and stress, respectively. Figs. 4-5 show the geometrical properties of the WPDs installed as diagonal bars, in the first and second stories respectively, of the test structure. Fig. 6 shows the test structure with the WPDs, with indication of the geometrical properties of the frames. Fig. 7 shows the connection of the damper on the frame structure, and Fig. 8 a scheme with the labels (D1, D2, D3, D4) assigned to the WPDs. The partial structural model was built at the Laboratory of Dynamics of Structures of the University of Granada (Spain). The WPDs were built with steel which yield stress, maximum stress and Young's modulus were 340MPa, 441MPa and 2.1×10^5 MPa, respectively. The yield stress of the steel used for reinforcing the concrete was 551MPa for the longitudinal rebars and 636 MPa for the stirrups. The concrete compressive strength on the 28th day was 35 MPa.

The auxiliary steel bars of each WPD (Figs. 4-5) were designed to be much stiffer under flexural and axial deformations than the I-sections. The auxiliary bars were moreover designed to remain elastic while the I-section steel segments underwent plastic deformations. The end-plates of the auxiliary bars of the WPDs were welded to steel plates anchored with corrugated bars to the RC members before concrete casting, as shown in Fig. 7. Given this configuration, when the frame moves laterally, the WPDs are basically subjected to axial forces N , i.e., acting in the direction of the axis of the damper, inducing axial deformations δ . The geometry of each I-section steel segment is shown in Fig. 9.

The 3D frame with the WPDs was placed on the uniaxial MTS 3×3 m² shaking table of the University of Granada (Spain) as shown in Fig. 6, and schematically in Fig. 10. The bottom ends of the columns were bolted to the table. Steel blocks were attached atop the slab and at the top of half columns of the second story. The total mass of the test structure (including the additional masses) was 12450 kg. The inertial mass located at the top of the test structure was 5970 kg. When the shaking table is accelerated, the inertial force generated in these steel blocks (inertial mass) and in the slab dynamically loads the WPDs, imposing axial forced deformations. The 3D frame with the WPDs was subjected to dynamic tests consisting of four seismic simulations, referred to as LH100, LH200, LH300 and LH350 hereafter, in which the shaking table reproduced the ground motion recorded at Calitri during the Campano Lucano (1980) earthquake, scaled in amplitude to 100%, 200%, 300% and 350%. The corresponding peak ground accelerations were 0.16 g, 0.31 g and 0.47 g and 0.54 g, respectively. Fig. 11 shows the time-history of the table motions in terms of acceleration. This ground motion was selected because its acceleration spectra which is shown in Fig. 12 is approximately flat in the vicinity and beyond the elastic period T of the test structure investigated. The histories of forced displacements imposed by these motions on dampers D1 and D3 are shown in Fig. 13. The histories of loading applied to dampers D2 and D4 were very similar to D1 and D3, respectively. These loading histories compare with the well-known basic loading history of the SAC protocol used for steel buildings in that: (i) in both cases there is a large number of cycles of similar amplitude; in other words, the history is not characterized by one very large excursion; and (ii) the cycles applied during the shaking table tests approach the symmetry in peak deformations of the SAC protocol.

The slab that formed the first floor and the steel blocks located at the top of half columns of the second story were instrumented with displacement transducers and accelerometers that measured the horizontal displacements and accelerations in the direction of the shaking and also in the perpendicular direction. The WPDs were instrumented with displacement transducers (indicated as LVDT in Figs. 4-5) that measured the axial deformations, and strain gages (indicated with a rectangle in Figs. 4-5) that allowed to calculate the axial force N sustained by each WPD during the history of loading. Since the auxiliary bars of the WPDs were very stiff and remained elastic, the relative displacement δ between the flanges of I-section steel segments was basically the same for all segments.

Prior to the shaking table tests and after each seismic simulation, free vibration tests were conducted to estimate the fundamental vibration period T_1 and the associated damping ratio ξ of the whole structure (with dampers). Both T_1 and ξ remained basically unchanged with the values of $T_1=0.21$ s, and $\xi=2.6\%$, this indicating that the dampers effectively prevented the main frame from damaging. The fundamental period of the bare frame (without dampers) fT_1 was also estimated giving $fT_1=0.6$ s. During the seismic simulations, the structure showed a strong column-weak beam mechanism. As a result, the maximum inter story drifts, expressed as a percentage of the story height, were almost the same in the first and second stories, the average values being 0.31% for

LH100, 0.61% for LH200, 1.02% for LH300 and 1.27% for LH350. The strains in the longitudinal reinforcement located at the base the columns of the first story reached $4.5\varepsilon_y$, where ε_y is the yield strain. In the rest of RC members, the strains at member end sections ranged from $0.4\varepsilon_y$ to $0.9\varepsilon_y$ in columns, and from $0.16\varepsilon_y$ to $0.23\varepsilon_y$ in beams.

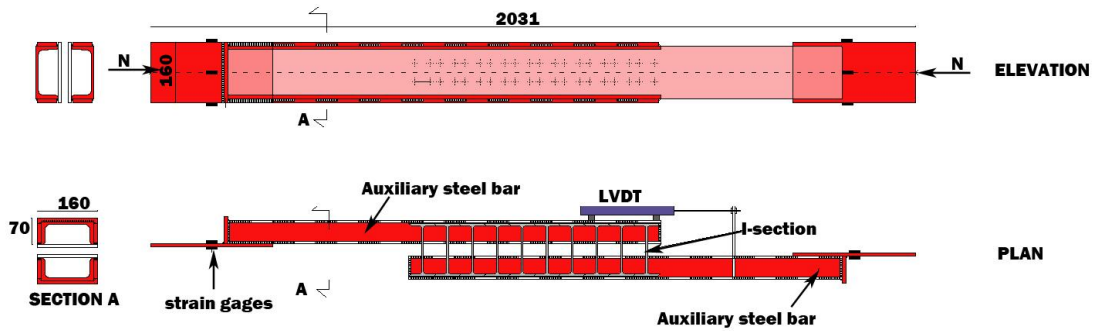


Fig. 4 WPD tested: lower dampers D1 and D2 (dimensions in mm)

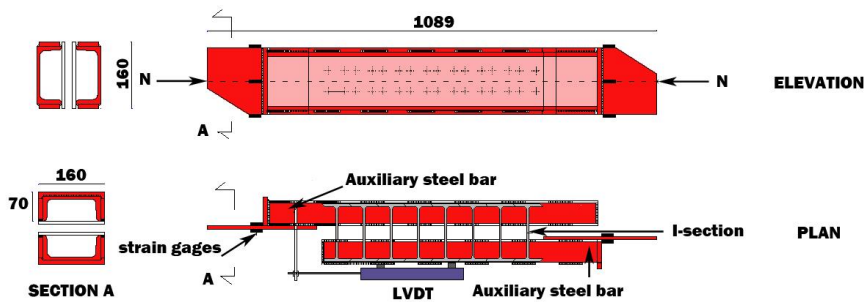


Fig. 5 WPD tested: upper dampers D3 and D4 (dimensions in mm)



Fig. 6 Test structure (dimensions in mm) and set-up



Fig. 7 Connection of the brace damper with the frame

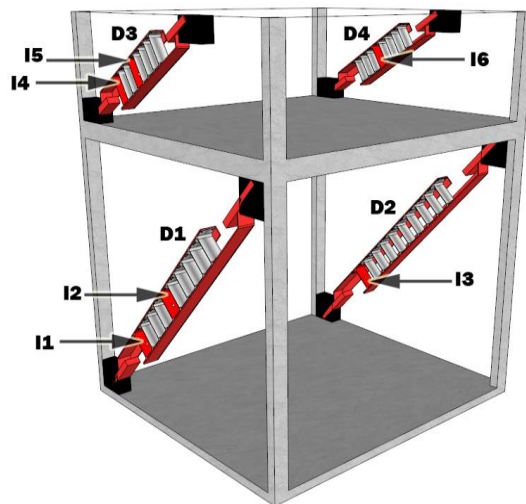


Fig. 8 Labels assigned to dampers (D1 to D4) and to the instrumented I-sections (I1 to I6)

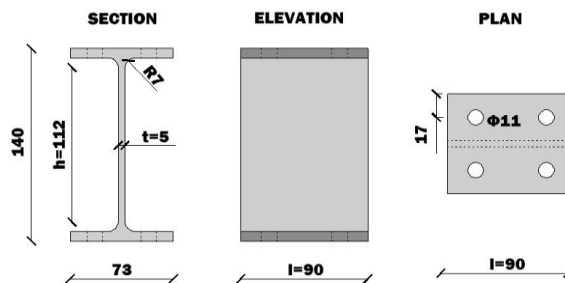


Fig. 9 Geometry of each I-section steel segment (dimensions in mm)

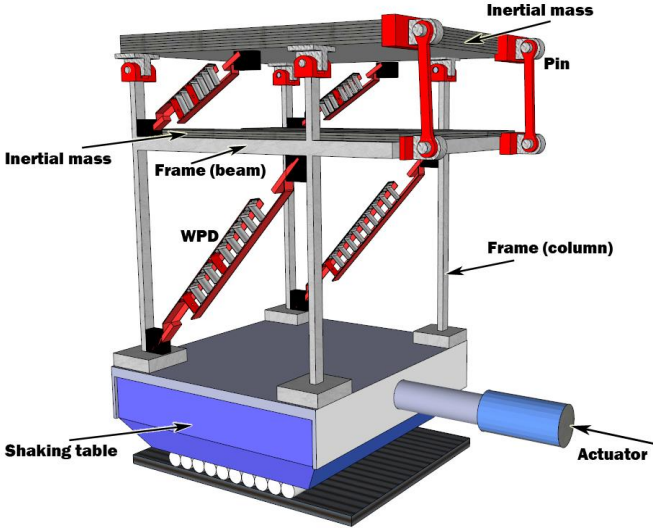


Fig. 10 Arrangement of the WPDs in the 3D frame

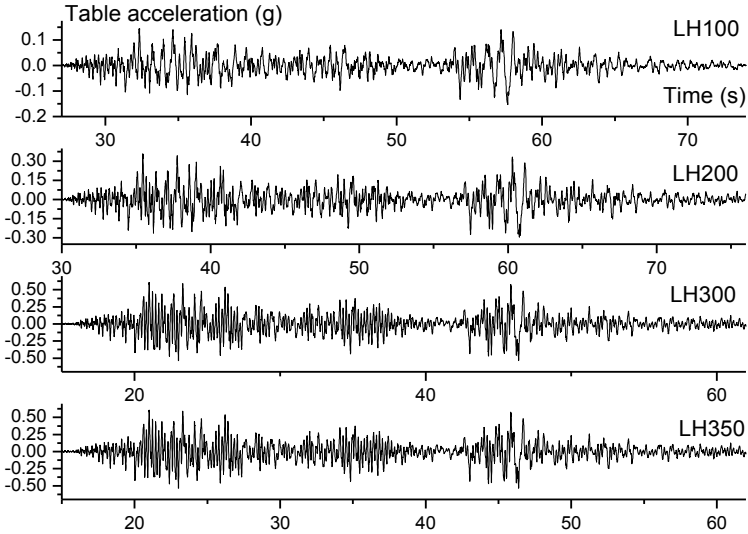


Fig. 11 Histories of accelerations applied to the shaking table

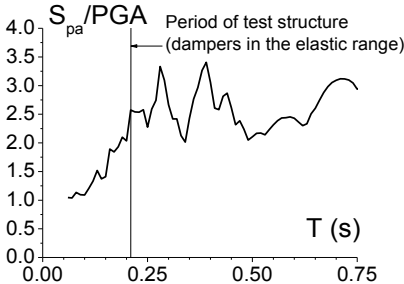


Fig. 12 Normalized acceleration spectra of the accelerogram used in the tests

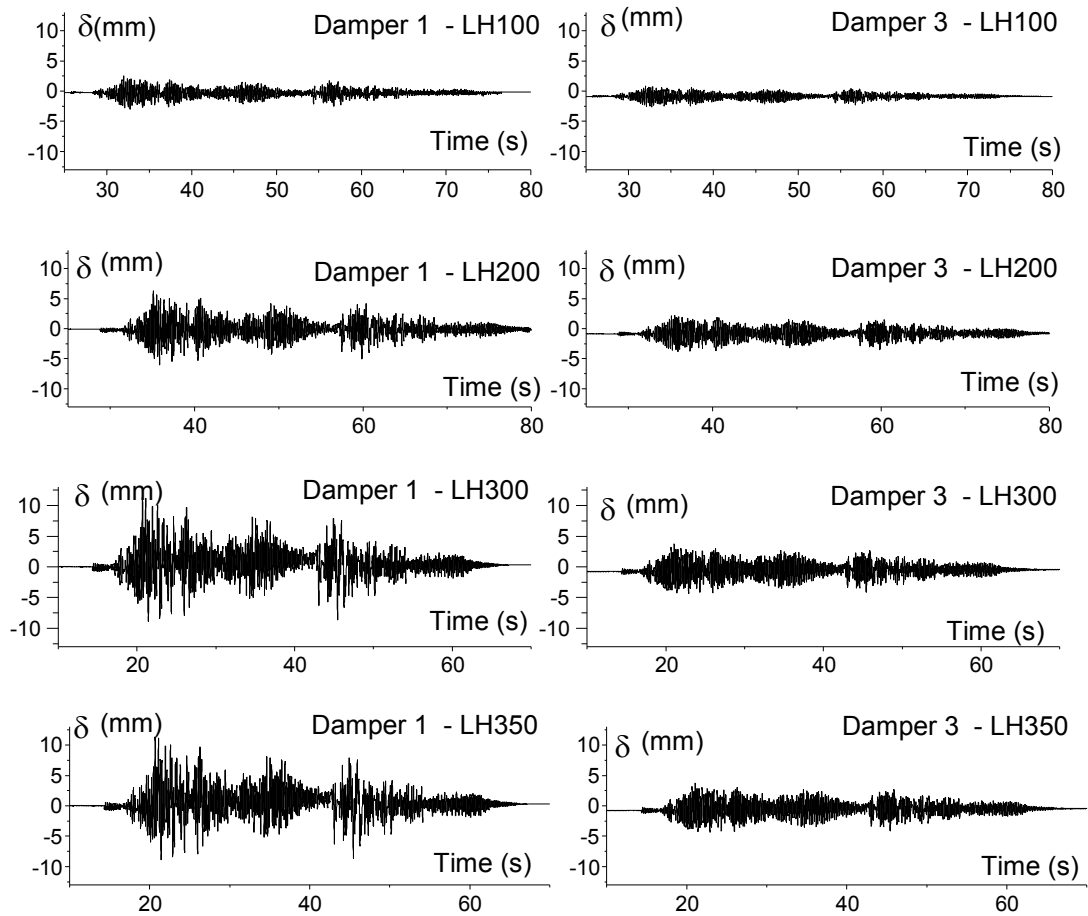


Fig. 13 Loading histories (imposed displacements) applied to the WPDs

2.2 Vibration tests conducted with piezoelectric ceramic actuators

Fig. 8 shows the distribution of the instrumented I-section steel segments on the WPDs. The lower dampers are denoted as D1 and D2, and the upper dampers as D3 and D4. Two I-sections were instrumented in dampers D1 and D3, while only one I-section was instrumented in dampers D2 and D4. Doubling the number of instrumented I-sections of dampers D1 and D3 served to evaluate the robustness of the health monitoring procedure. That is, since all I-sections of the same damper share similar geometry and material properties, and they are subjected to the same history of imposed deformations, and if the procedure for its evaluation is robust enough, for a given level of damage the index AID on the two I-sections of the same WPD should be very similar. The position and name (I1, I2, I3, I4, I5, I6) of the instrumented I-sections can be seen in Fig. 8.

The instrumentation consisted of attaching piezoelectric ceramic sensors to the web -one PZT model PI® PRYY0842 working as the actuator attached right at the centre of the I-section web, and one PZT model PI® PRYY+0220 serving as a sensor just opposite the other, as shown in Fig.

14. Both sensors were located in the central part of the web of the I-section because the level of deformation in this region is minimal (nominally zero bending moment), and this prevents the PZTs from breaking. Also, past research (Romo-Melo 2012) revealed that in this area the sensor is able to detect all the resonant frequencies. Fig. 15 shows the connections between the PZTs and the electronic measurement system up to the workstation.

Both sensors and actuators were provided with shielded C-202 cable and housing Molex connectors for their interconnection with interface boxes, which impede undesirable effects caused by the movement of cables during dynamic testing. Also, they allow for adapting individual sensor terminals with a RJ-45 connector for simultaneous signal transmission to a distribution box by means of a Category 6-Shielded STP cable. In the distribution box the signals are separated and connected to the data acquisition system by means of coaxial cables.

Electronic equipment consisted of two PULSE 3560-B *Bruel & Kjaer* systems for signal acquisition, a *Coco80 Crystal Instrument* as the generator system, an amplifier EPA104 of *PiezoSystem* and other auxiliary box interfaces as indicated in Fig. 15. PULSE 3560-B is an acquisition system configured to obtain the sensor signals simultaneously in differential mode to avoid the electronic noise and any electromagnetic interference. The CoCo80 system was used to produce the electrical signal to excite the PZT actuators. The white noise signal was selected as the

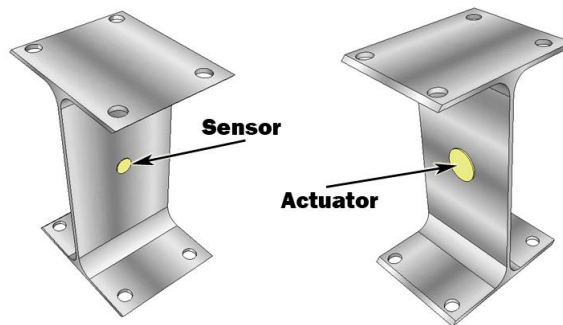


Fig. 14 I-section instrumentation: sensor and actuator

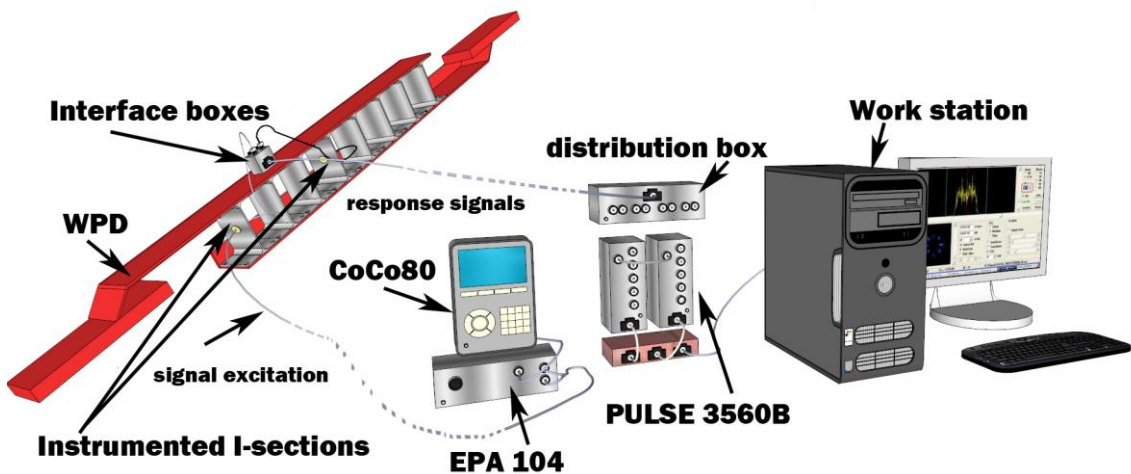


Fig. 15 Scheme of electronic measurement system

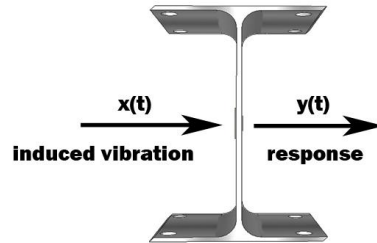
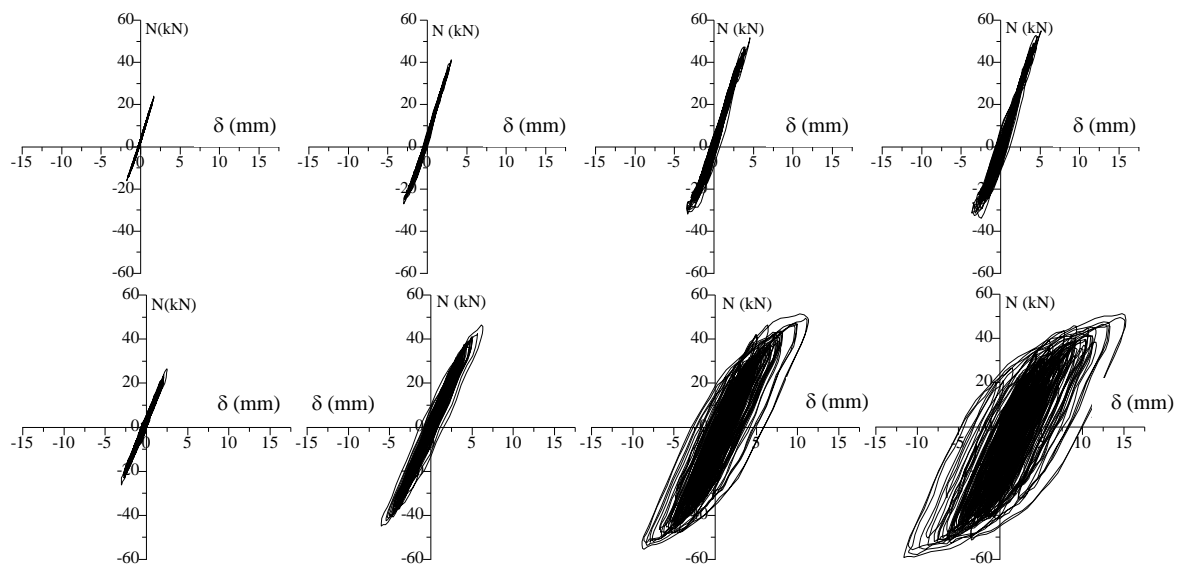


Fig. 16 Vibration test on I-sections with PZTs

Fig. 17 N - δ curves of dampers D1 (1st row) and D3 (2nd row) corresponding to seismic simulations LH100 (1st column), LH200 (2nd column), LH300 (3rd column), LH350 (4th column)

most appropriate excitation for these experiments, as shown in previous research (Romo-Melo 2012). The maximum amplitude of signal produced for the CoCo80 was 10 Vpp, insufficient to adequately excite the I-sections; it was therefore necessary to use the EPA104 piezoelectric amplifier to provide power performance to excitation. The amplifier provided a gain of 20 to arrive at an amplitude of about 200 Vpp. All electronic devices were properly connected to the grounding system and connections were made so that the measurement system would have good performance against the electrical and environmental noises. Thus, a robust measurement system was obtained, with controlled noise conditions and high quality vibration signals.

Vibration tests were induced vibrations, $x(t)$, conducted on each instrumented I-section by means of the PZT actuator attached at the center of the web and measuring the signal response, $y(t)$, through the PZT sensor adhered on the opposite side of the I-section web as shown in Fig. 16.

Vibration tests were conducted after each history of dynamic cyclic loading LH100, LH200, LH300 and LH350. For statistical purposes, each vibration test was carried out five times with different white noise realizations. The duration of each test was 20 seconds, and the rate of signals was 65.536 samples per second. In general, the voltage amplitude obtained by PZT sensors was

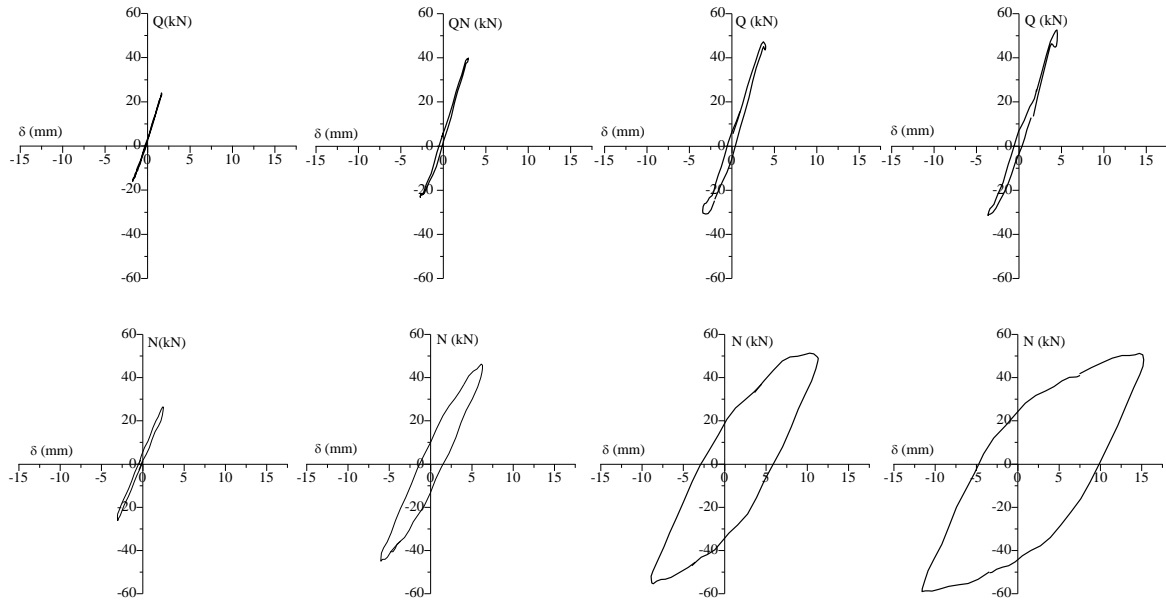


Fig. 18 N - δ curves at maximum drift of dampers D1 (1st row) and D3 (2nd row) during seismic simulations LH100 (1st column), LH200 (2nd column), LH300 (3rd column), LH350 (4th column)



Fig. 19 Close-up views of the deformed web at the maximum drift

around 3 to 4 V. The total number of time signals acquired during the vibration tests was 120, corresponding to the six instrumented I-sections, five white noise realizations and four loading histories. All signals were acquired with the maximum useful frequency range, 26 kHz, permitted by the acquisition system.

3. Behavior of the dampers under cyclic loadings

The axial force-displacement, N - δ , loops recorded in the hysteretic dampers were similar for the two dampers located in the same story. Fig. 17 shows the N - δ loops of dampers D1 and D3.

The first row of graphs corresponds to damper D3 and the second row to damper D1; the 1st, 2nd, 3rd and 4th columns of graphs correspond to seismic simulations LH100, LH200, LH300 and LH350, respectively. For the same dampers and seismic simulations, Fig. 18 shows the N - δ curves at maximum drift. Fig. 19 shows close-up views of the deformed web at the maximum drift.

4. Experimental results: mechanical damage index ID

4.1 Decomposition of the N - δ curves

The typical (idealized) axial load-displacement N - δ curve measured with the strain gages and the displacement transducer LVDT in each WPD during each history of loading is of the type shown in Fig. 20.

The N - δ curve exhibited by a WPD up to a given level of damage D_i is defined by point i of the coordinates (N_i, δ_i) , and it can be decomposed into the so-called skeleton part (Fig. 21) and the Bauschinger part (Fig. 22)

The skeleton part (Fig. 21) is formed by connecting sequentially the segments 0-1, 5-6, 11-12, and 17-18 in the positive domain, and 2-3, 8-9, and 14-15 in the negative domain -which are the paths that exceed the load level attained by the preceding cycle in the same domain of loading. Segments 1-2, 6-7, 12-13, 18-19, 3-4, 9-10, and 15-16 are the unloading paths, whose slope

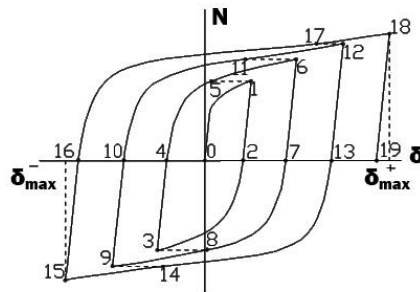


Fig. 20 Typical axial load-displacement N - δ curve

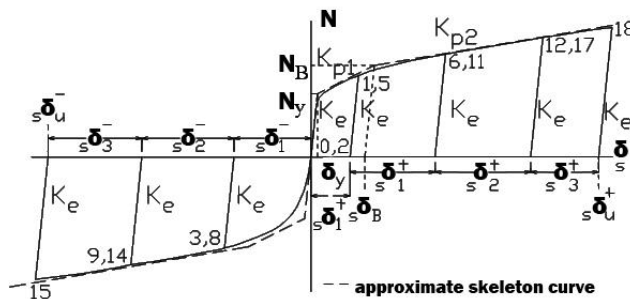


Fig. 21 Decomposition of a typical N - δ curve in the skeleton part

coincides with the initial elastic stiffness $K_e=N_y/\delta_y$, where N_y and δ_y are the axial force and the axial displacement at yielding. In each domain of loading, the area enveloped by the skeleton curve up to a given point (N_i, δ_i) will be called ${}_sW_i^+$ and ${}_sW_i^-$. The segments 4-5, 10-11, and 16-17 in the positive domain, as well as 7-8 and 13-14 in the negative domain of loading -which begin at $N=0$ and terminate at the maximum load level previously attained in preceding cycles in the same loading domain- are the so-called Bauschinger part (Fig. 22).

In each domain of loading, the sum of the areas enveloped by the Bauschinger part up to a given point (N_i, δ_i) will be referred to as ${}_B W_i^+$ and ${}_B W_i^-$. The sum ${}_sW_i^+ + {}_B W_i^+$ in the positive domain, and ${}_sW_i^- + {}_B W_i^-$ in the negative domain, is the total plastic strain energy dissipated by the WPD in each domain of loading. For convenience, these energies can be expressed in non-dimensional form in terms of the new ratios ${}_s\bar{\eta}_i^+, \bar{\eta}_i^+, {}_s\bar{\eta}_i^-, \bar{\eta}_i^-$ defined as follows

$${}_s\bar{\eta}_i^+ = \frac{{}_sW_i^+}{N_y \delta_y}; \quad \bar{\eta}_i^+ = \frac{{}_sW_i^+ + {}_B W_i^+}{N_y \delta_y}; \quad {}_s\bar{\eta}_i^- = \frac{{}_sW_i^-}{N_y \delta_y}; \quad \bar{\eta}_i^- = \frac{{}_sW_i^- + {}_B W_i^-}{N_y \delta_y} \quad (1)$$

The level of strains induced in the WPDs during each seismic simulation can be characterized in terms of the maximum plastic deformation attained by the WPDs on the skeleton part in each domain of loading, ${}_s\delta_u^+$ and ${}_s\delta_u^-$, normalized by the yield deformation δ_y . The values of ratios ${}_s\delta_u^+/\delta_y, {}_s\delta_u^-/\delta_y$ are shown in Table 1. It can be derived from Table 1 that during the seismic simulation LH100 the strains in the web of the I-sections of dampers D3 and D4 remained below the yield strain, while those of dampers D1 and D2 exceeded the yield strain. For the subsequent seismic simulations, the strains in the web of the I-sections of all dampers reached the plastic range and were about 3-4 times larger for dampers D1 and D2 than for dampers D3 and D4.

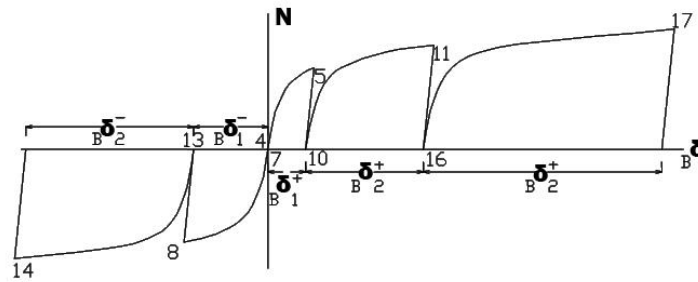


Fig. 22 Decomposition of a typical N-δ curve in the Bauschinger part

Table 1 Plastic deformation level on the dampers

Loading histories	Damper D1		Damper D2		Damper D3		Damper D4	
	${}_s\delta_u^+/\delta_y$	${}_s\delta_u^-/\delta_y$	${}_s\delta_u^+/\delta_y$	${}_s\delta_u^-/\delta_y$	${}_s\delta_u^+/\delta_y$	${}_s\delta_u^-/\delta_y$	${}_s\delta_u^+/\delta_y$	${}_s\delta_u^-/\delta_y$
LH100	1.6	1.5	2.6	2.5	0.79	0.75	0.78	0.88
LH200	3.5	3.6	5.5	5.2	1.8	1.4	1.7	1.6
LH300	5.7	6.4	7.9	8.3	2.6	2.1	2.1	2.6
LH350	5.7	8.8	11	9.2	3.0	2.5	2.2	3.0

Table 2 Mechanical damage index- ID_i for all dampers

Loading histories	Lower dampers		Upper dampers	
	D1	D2	D3	D4
LH100	0	0	0	0
LH200	0.17	0.12	0.03	0.03
LH300	0.45	0.42	0.07	0.06
LH350	0.77	0.78	0.12	0.12

4.2 Evaluation of mechanical damage through the energy-based index ID_i

Past research (Benavent-Climent 2007) showed that the level of mechanical damage in a metallic EDD subjected to arbitrarily applied cyclic loading up to a point (N_i, δ_i) can be accurately predicted by the following index

$$ID_i = \max\{\overline{ID}_i^+, \overline{ID}_i^-\} \quad (2)$$

where

$$\overline{ID}_i^+ = \frac{\overline{\eta}_i^+}{\overline{\eta}_u^+}, \quad \overline{ID}_i^- = \frac{\overline{\eta}_i^-}{\overline{\eta}_u^-} \quad (3)$$

In Eq. (3), $\overline{\eta}_u^+$ and $\overline{\eta}_u^-$ represent the ultimate energy dissipation capacity of the hysteretic damper, depending on the values of ${}_s\overline{\eta}_i^+, \overline{\eta}_i^+, {}_s\overline{\eta}_i^-, \overline{\eta}_i^-$ and on two empirical parameters a and b related to the material properties of the steel and the geometry of the damper. A detailed explanation of these parameters and their value for the type of damper investigated in this study can be found in reference (Benavent-Climent *et al.* 2011a).

The value $ID_i=0$ indicates no damage, while $ID_i=1$ means complete failure. Table 2 shows the value of the mechanical index ID_i calculated for the four dampers D1, D2, D3 and D4 from the N - δ curve obtained during each history of loading. It can be seen that, after the last loading history LH350, the lower dampers (D1, D2) were very close to failure (i.e., ID is close to 1), while the upper dampers were slightly damaged.

5. Experimental results: area index of damage aid

For detection and evaluation of different levels of damage in the I-sections of dampers during the seismic simulations, the signals of the vibration tests were processed using the procedure described by the authors in previous research (Benavent-Climent *et al.* 2014, Gallego *et al.* 2012). This process provided a vibration index, AID, which is based on the frequency response function of time vibration signals. AID is a quantitative estimation of damage intended specifically to measure the health of I-sections in WPD dampers. The index is rooted in a physical principle according to which changes in the physical properties of a structure or structural element likewise change its vibrational response (Rytter 1993, Romo-Melo 2012). Thus, the method relies on a direct correlation between the changes in the vibrational response of a structure and the presence

of damage (Dawson 1976, Doebling *et al.* 1998).

5.1 Frequency representation - FRF

Calculation starts with a correct representation of the data after suitable normalization (Benavent-Climent *et al.* 2014). For this application, the magnitude of the FRF estimate was obtained following the mathematical representation presented in this equation

$$|\hat{H}(j\omega)| = \frac{|XY(j\omega)|}{\hat{X}(\omega)} \tag{4}$$

where $XY(j\omega)$ and $\hat{X}(\omega)$ are the cross and auto-spectral density functions of response and excitation signals, respectively, estimated via the Welch method, as explained in (Benavent-Climent *et al.* 2014, Kay 1988). Fig. 23 shows the estimated FRF magnitude (in dB) of vibration tests conducted in each of the six instrumented I-sections after loading history LH100.

As can be seen in Fig. 23, the frequency response was very similar for all the I-sections tested. That is, although all I-sections exhibit similar resonance peaks, each I-section has its own resonance frequency. The differences between the FRF spectra of each I-section are due to small deviations of their actual geometry from the nominal one. The material properties of all I-section steel segments were the same, having been cut from the same bar.

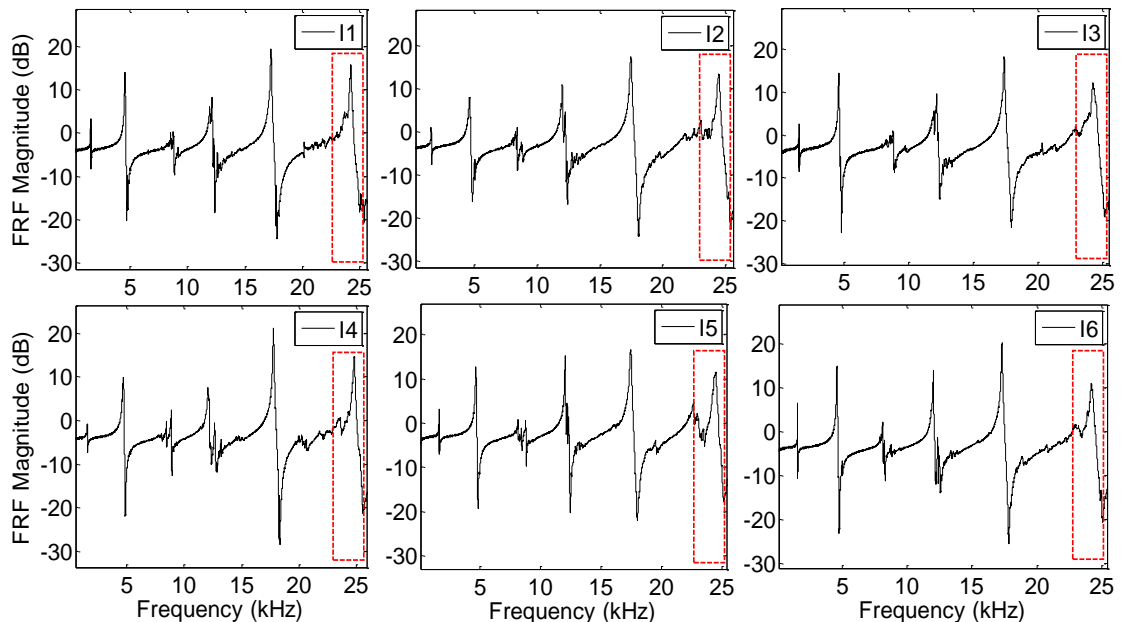


Fig. 23 Magnitude of FRF estimates for the six I-sections after loading history LH100, and for the first white noise realization

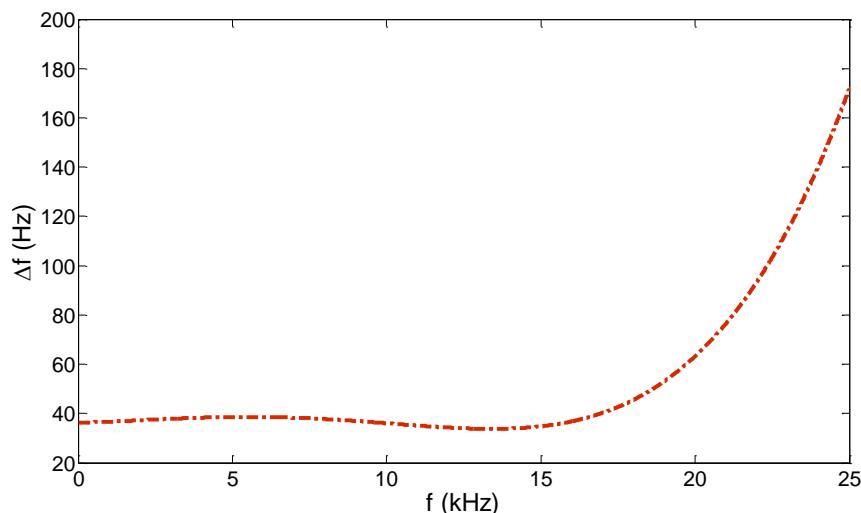


Fig. 24 Maximum frequency shift (Δf) of resonances (f) of I-section until ultimate energy dissipation capacity is attained

5.2 Bandwidth selection and data filtering

Once the resonance peaks of the I-sections had been determined, the next step was to select the most appropriate bandwidth for damage detection. To this end we relied on results from previous tests, applying quasi-static loads to several I-sections until their ultimate capacity of energy absorption (Benavent-Climent *et al.* 2014). These experiments showed that the damage is more clearly detectable at highest frequencies. Accordingly, the resonant peak frequency bandwidth selected for evaluating the damage was the highest one, as indicated within a box in Fig. 23.

The results of previous tests (Benavent-Climent *et al.* 2014) provided further information on the maximum frequency shift Δf that the resonant peaks of an I-section can experience before it attains its ultimate energy dissipation capacity and fails. This information is plotted in Fig. 24, where the horizontal axis represents the resonant peak frequency f of the undamaged I-section, and the vertical axis Δf . This curve can be expressed by the following polynomial equation

$$\Delta f = 1.5e - 15f^4 - 3.7e-11f^3 + 1.9e-07f^2 + 2.3e-04f + 36.3 \quad (5)$$

Thus, knowing the resonance peak frequencies of the healthy I-section and using Eq. (5), it is possible to approximate the maximum frequency shift that can be expected at each resonant peak. The curve shows that for the lowest frequencies, between 0 and 15 kHz, the maximum frequency shift is low and almost constant, approximately 40 Hz. This low frequency shift makes the damage hardly detectable around these resonant frequencies. However, for resonant peak frequencies above 15 kHz, Δf grows exponentially, making the damage more easily detectable. For this reason, in the present research only the highest resonant peak frequencies were considered. Accordingly, the bandwidth (BW) for each instrumented I-sections was selected considering only its highest resonance frequency, f , the expected frequency shift predicted with Eq. (5), Δf , and a scale factor, Q , that governs the width of the spectra at both sides of the resonance frequency, i.e.,

$$BW = [f - Q \Delta f , f + Q \Delta f] \tag{6}$$

In this study, a scale factor of $Q=3$ was used. Table 3 shows f , Δf and BW obtained for each I-section, whereas Fig. 25 gives the FRF estimate magnitude, in dB, obtained for each in the four histories of loading.

I-sections I1, I2 and I3 corresponding to the lower dampers D1 and D2 experienced more significant frequency shifts than I3, I4 and I5, placed in the upper dampers (Fig. 25). This observation is consistent with the fact that the mechanical damage (as measured by ID) in the lower dampers was more severe than in the upper dampers, as discussed below. The frequency shifts of pair I1 and I2 installed in damper D1, and pair I4 and I5 installed in damper D3 are seen to be similar, consistent with the fact that they were installed in the same damper.

Table 3 Resonance frequency f , maximum frequency shift Δf , and bandwidth BW of analysis, for each I-section

I-section	Resonance f (Hz)	Maximum Shift Δf (Hz)	Analysis bandwidth BW (Hz)
I1	24243	148	[23.800–24.686]
I2	24531	157	[24.061–25.001]
I3	24340	151	[23.888–24.792]
I4	24831	166	[24.333–25.329]
I5	24469	155	[24.006–24.933]
I6	24305	149	[23.857–24.753]

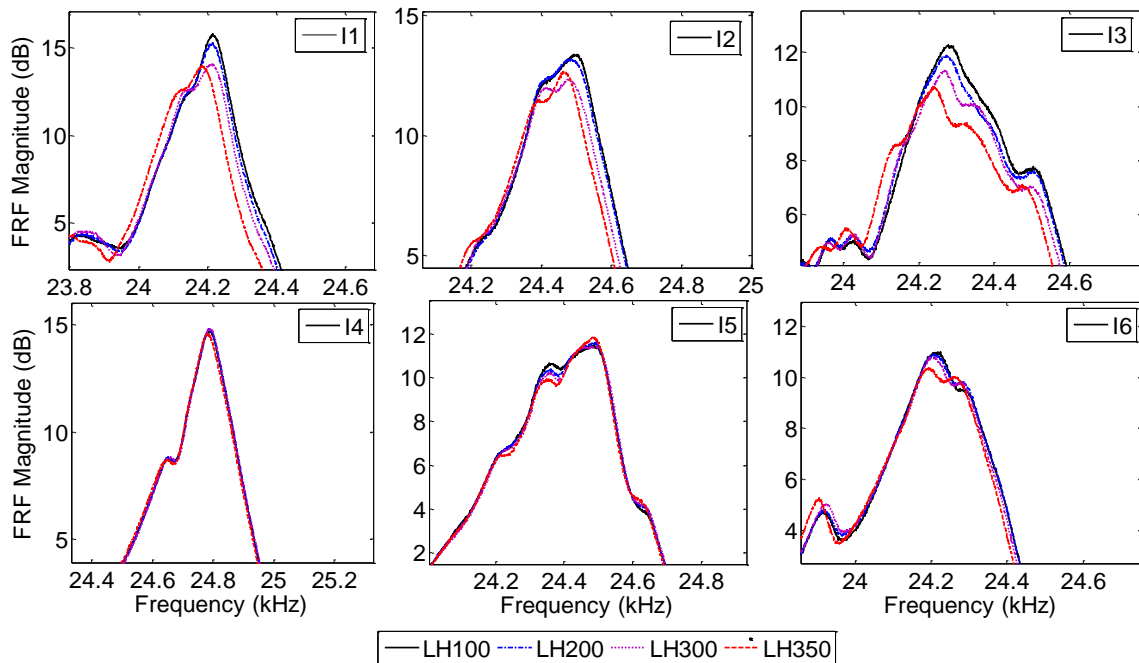


Fig. 25 FRF magnitude estimate (dB) on selected bandwidth for the six I-sections during each seismic simulation

5.3 Non-parametric statistical test

A non-parametric statistical test method based on the FRF magnitude was applied to the filtered vibration signals. The $|Z|$ -statistics magnitude was obtained following the procedure suggested in (Benavent-Climent *et al.* 2014, Gallego *et al.* 2012), using this Equation

$$|Z| = \frac{\delta |\hat{H}(j\omega)|}{\sqrt{2\hat{\sigma}_0^2(\omega)}} \quad (7)$$

where

$$\delta |\hat{H}(j\omega)| = \left| \hat{H}_0(j\omega) \right| - \left| \hat{H}_u(j\omega) \right| \quad (8)$$

$\delta |\hat{H}(j\omega)|$ being the difference between the FRF estimated for the I-section taken as reference, $|\hat{H}_0(j\omega)|$, typically the healthy state, and the FRF estimated for the inspection I-section, $|\hat{H}_u(j\omega)|$, typically the faulty state. Then, $\hat{\sigma}_0^2(\omega)$ is the variance of $|\hat{H}_0(j\omega)|$, (Gallego *et al.* 2012, Fassois and Sakellariou 2007). In the experiments conducted in this study, the mechanical damage on the dampers after the loading history LH100 was non-existent, since the maximum axial deformation on the dampers was below the yielding deformation δ_y and therefore they remained in the elastic range.

Hence, the state of each I-section after applying the loading history LH100 was taken as the reference “healthy state”. Signals measured after successive histories of loadings LH200, LH300 and LH350 were taken as the inspection states for each I-section. Fig. 26 presents the $|Z|$ -statistic magnitudes obtained for I-sections placed on lower dampers D1 and D2, and Fig. 27 those of upper dampers D3 and D4.

Since the lower dampers suffered greater mechanical damage than the upper ones (as discussed later with the index ID), the lower I-sections of the lower dampers (I1, I2 and I3) exhibit a $|Z|$ -statistic much greater than that of I4, I5 and I6. Moreover, the area of $|Z|$ -statistic grows along with the level of damage. This makes it possible to apply the criteria used to calculate the Area Index of Damage, or AID (Benavent-Climent *et al.* 2014, Gallego *et al.* 2012).

5.4 AID calculation

To estimate quantitatively the level of damage suffered by the instrumented I-sections after each loading history (LH100, LH200, LH300 and LH350), damage index AID, based on the analysis of signals of vibration tests, was proposed by the authors in previous research (Benavent-Climent *et al.* 2014). The index AID is defined as follows

$$AID = \int_{\omega_{\min}}^{\omega_{\max}} |Z|(\omega) d\omega \quad (9)$$

where $|Z|(\omega)$ represents the $|Z|$ -statistic magnitude in the frequency (ω). Table 4 presents the AID values for each damage level calculated for the six instrumented I-sections on the selected bandwidth, while Fig. 28 shows the representation of AID against the damage levels.

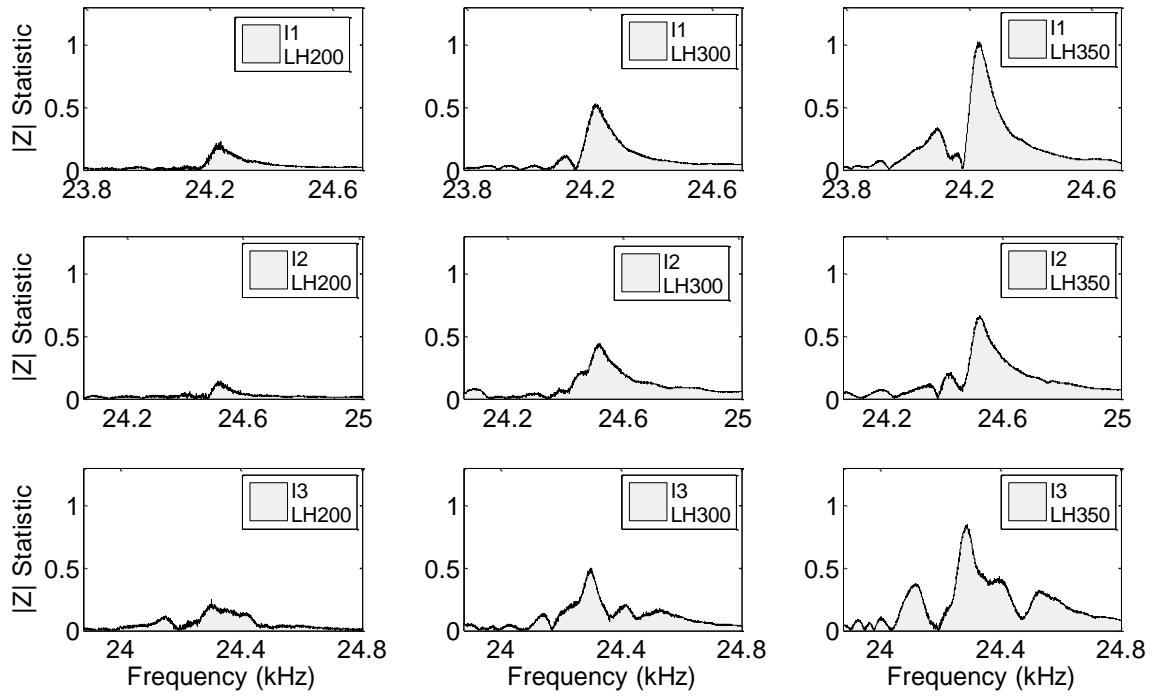


Fig. 26 |Z|-statistic magnitudes for all damage states on I-sections located on lower dampers

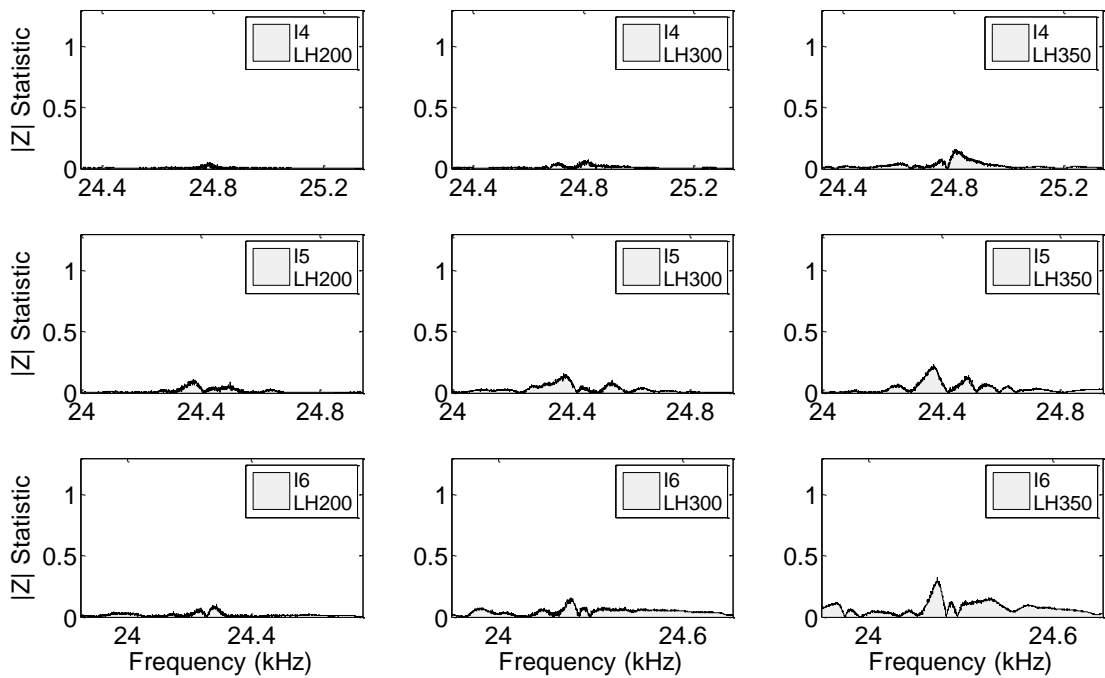


Fig. 27 |Z|-statistic magnitudes for all damage states on I-sections located on upper dampers

Table 4 AID calculated for each I-section

LH	D1		D2	D3		D4
	I1	I2	I3	I4	I5	I6
100	0	0	0	0	0	0
200	64,8	45,9	95,4	9,8	25,3	27,3
300	169,9	195,7	196,5	21,6	50,1	75,7
350	354,1	283,5	391,6	51,4	68,6	129,8

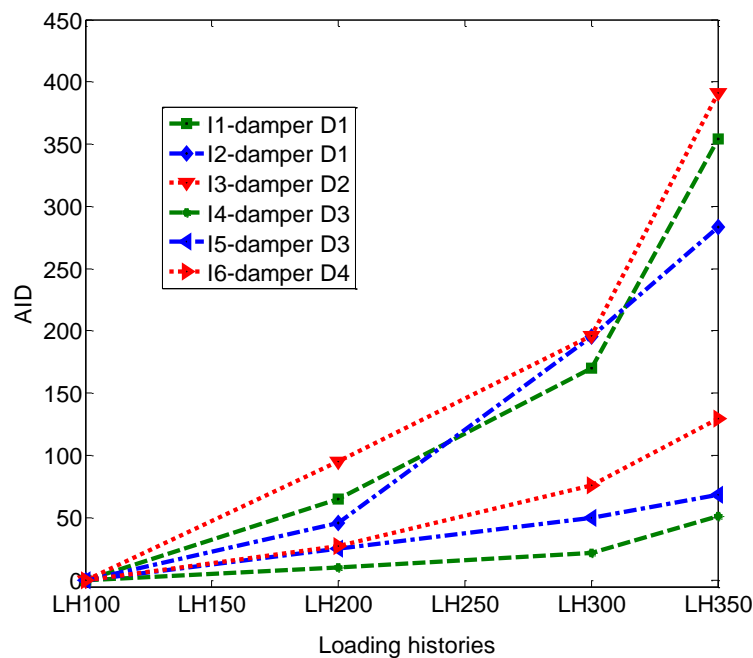


Fig. 28 AID values against damage levels of seismic simulation for the six I-sections

Note that the damage in terms of AID of the I-sections mounted in the lower dampers D1 and D2 (I1, I2 and I3) experienced nearly exponential growth with the amplitude of the applied history of loading. These results are consistent with those obtained using the mechanical index ID. The I-sections located on the lower dampers exceed 300 units of AID, while in I4, I5 and I6, in the upper dampers, damage is barely noticeable.

6. Correlation between ID and AID

Previous experiments applying cyclic static loads (Benavent-Climent *et al.* 2014) showed that it is possible to establish a good linear relationship between the mechanical index ID and the vibration based damage index AID calculated for high frequency bands. In this section, the conclusion reached from the static cyclic tests is assessed for dynamic cyclic loadings, a more realistic loading condition in the case of earthquakes. Table 1 in section 3 shows the mechanical

damage index ID for the six instrumented I-sections, and Table 2 in section 6.4. gives the corresponding AID values. It is worth recalling that, since index ID is calculated from the overall axial load-displacement curve $N-\delta$ of the WPD, which includes the response of all the I-section steel segments connected in parallel, there is a single and common ID value for all the I-sections mounted in the same WPD. In contrast, the index AID is calculated individually for each I-section of the WPD.

Fig. 29 illustrates the good correlation between damage index ID and AID for each damper separately. Furthermore, the relation between AID and ID is almost linear and can be approximated by the following simple equation

$$ID = 0.002 AID \tag{10}$$

The above Eq. (10) provides a very close estimation of the mechanical damage (in terms of ID) from index AID for dampers D1, D2 and D3, and a safe-side estimation of the damage for damper D4. Extrapolating the tendency given by Eq. (10), failure of the WPD can be expected when AID=500. It is also noteworthy that the AID obtained for the two I-sections mounted in the same WPD (I1 and I2 for damper D1, and I4 and I5 for damper D3) are close and of the same order of magnitude. Since all the I-sections installed in the same WPD experience similar mechanical damage, this result proves the robustness of the health monitoring technique based on vibration tests described in this study.

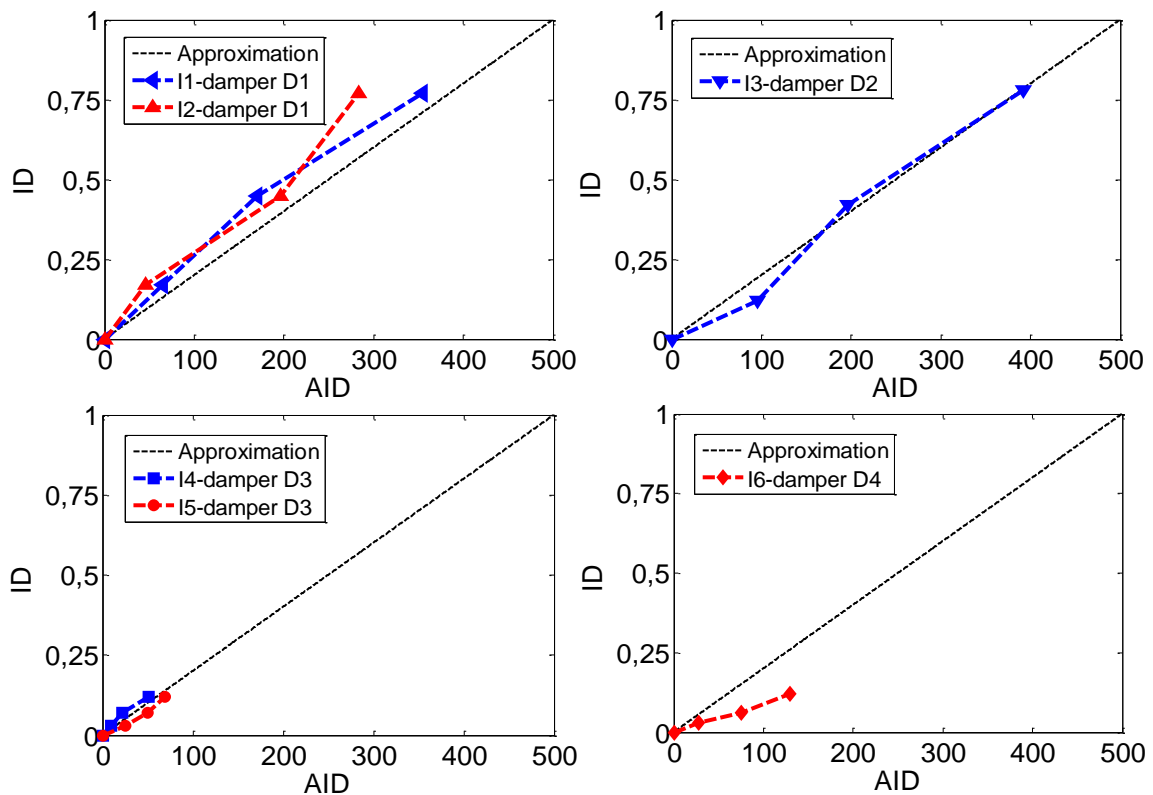


Fig. 29 ID vs. AID for each damper

7. Conclusions

This study experimentally investigates a health monitoring technique to quantify the damage in hysteretic dampers subjected to dynamic cyclic loadings of the type imposed by earthquakes. The damper investigated (called WPD) consists of segments of I-section steel profiles arranged in a brace-type configuration, so that they work in series when the WPD is subjected to forced deformations in the axial direction. The health monitoring technique uses non-parametric statistical processing of the excitation and response signals obtained from simple vibration tests conducted with two piezoelectric ceramic sensors glued to the web of the I-section steel segments. The signals obtained from the vibration tests are processed with a Frequency Response Function method. Damage is detected from the changes in the frequency response of the specimen. A feature quantity Q is obtained from the FRF that makes it possible to calculate a new index, AID, found to be sensitive to the level of damage to the damper. The index AID is compared with a mechanical index ID previously proposed in the literature, calibrated based on the actual damage observed in dampers.

By subjecting four WPDs to dynamic cyclic loadings on a shaking table, earthquakes of increasing intensity were simulated, with four histories of loading (imposed deformations). After each loading history, simple vibration tests were conducted in six I-section steel segments mounted on the WPDs. From the axial force-axial displacement N - δ curve measured during each history of loading in each WPD, the corresponding mechanical damage index ID was determined, and the vibration-test based damage index AID was calculated from the signal. Comparison of the values of ID and AID for the same level of damage leads us to conclude that:

i) The simple linear relationship between ID and AID observed in past research, when the WPD was subjected to static cyclic loads, is likewise seen when applying the loads dynamically, as during an earthquake.

ii) The instrumentation proposed for conducting the vibration tests and the technique developed to process the signal and obtain AID is robust. This means that the same level of damage in two different I-section steel segments provides similar values for the AID.

iii) A simple formula is proposed to derive ID from AID. This makes it possible to precisely monitor the level of damage or proximity to failure of WPDs when subjected to dynamic loading representative of an earthquake, using simple vibration tests rather than cumbersome and expensive instrumentation on the damper.

Acknowledgements

This research received the financial support of the local government of Spain, *Consejería de Innovación, Ciencia y Tecnología*, Projects P07-TEP-02610 and P08-TEP-03641. The authors thank to Dr. Andrés Roldán for his support during the WPDs instrumentation and SHM experimental setup.

References

- Benavent-Climent, A. (2007), "An energy based damage model for seismic response of steel structures", *Earthq. Eng. Struct. Dyn.*, **36**, 1049-1064.

- Benavent-Climent, A., Morillas, L. and Vico, J. (2011a), "A study on using wide-flange section web under out-of-plane flexure for passive energy dissipation", *Earthq. Eng. Struct. Dyn.*, **40**(5), 473-490.
- Benavent-Climent, A. (2011b), "An energy-based method for seismic retrofit of existing frames using hysteretic dampers", *Soil Dyn. Earthq. Eng.*, **31**, 1385-1396.
- Benavent-Climent, A., Gallego, A., Romo-Melo, L. and Morillas, L. (2014), "Health monitoring of hysteretic dampers subjected to cyclic loading through vibration tests", *Struct. Health Monit.*, **13**, 33-49.
- Black, C.J., Makris, N. and Aiken, I.D. (2004), "Component testing, seismic evaluation and characterization of buckling-restrained braces", *J. Struct. Eng.*, **130**(6), 880-894.
- Christopoulos, C. and Filiatrault, A. (2006), *Principles of passive supplemental damping and seismic isolation*, IUSS Press, Pavia, Italy.
- Dawson, B. (1976), "Vibration condition monitoring techniques for rotating machinery", *Shock Vib. Dig.*, **8**(12), 3.
- Doebling, S., Farrar, C., Prime, M. and Shevitz, D. (1998), "A review of damage identification methods that examine changes in dynamic properties", *Shock Vib. Dig.*, **30**(2), 91-105.
- Fassois, S. and Sakellariou, J. (2007), "Time series methods for fault detection and identification in vibrating structures", *R. Soc. Philos. Tran.: Math. Phys. Eng. Sci.*, **365**, 411-448.
- Gallego, A., Benavent-Climent, A. and Romo-Melo, L. (2012), "Piezoelectric sensing and non-parametric statistical signal processing for health monitoring of hysteretic dampers used in seismic-resistant structures", *Mech. Syst. Sig. Proc.*
- Goulet, C.A., Haselton, C.B., Mitrani-Reiser, J., Beck, J.L., Dierlein, G.G., Porter, K.A. and Steward, J.P. (2007), "Evaluation of the seismic performance of a code-conforming reinforced-concrete frame building-from seismic hazard to collapse safety and economic losses", *Earthq. Eng. Struct. Dyn.*, **36**, 1973-1997.
- Gray, M.G., Christopoulos, C. and Packer, J.A. (2010), "Cast steel yielding fuse for concentrically braced frames", *Proceedings of the 9th U.S. National and 10th Canadian Conference on Earthquake Engineering*, Toronto, Canada.
- Housner, G., Bergman, L., Caughey, T., Chassiakos, A., Claus, R., Masri, S., Skelton, R., Soong, T. and Spencer, B. (1997), "Structural control: Past, present, and future", *J. Eng. Mech.*, **9**(123), 897-958.
- Kay, S. (1988), *Modern spectral estimation: Theory and application*, Englewood Cliffs, Prentice Hall, NJ.
- Kampas, G. and Makris, N. (2012), "Time and frequency domain identification of seismically isolated structures: advantages and limitations", *Earthq. Struct.*, **3**(3), 249-270.
- Konstantinidis, D., Makris, N. and Kelly, J.M. (2012), "Health monitoring of fluid dampers for vibration control of structures: experimental investigation", *Earthq. Eng. Struct. Dyn.*, **41**(13), 1813-1829.
- Makris, N. and Kampas, G. (2013), "The engineering merit of the 'effective period' of bilinear isolation systems", *Earthq. Struct.*, **4**(4), 397-428.
- Palermo, M., Silvestri, S., Gasparini, G. and Trombetti, T. (2014), "Crescent shaped braces for the seismic design of building structures", *Mater. Struct.*, 1-18.
- Romo-Melo, L. (2012), "Health monitoring of health monitoring of WPD-type hysteretic dampers used for passive control of earthquake resistant structures by means of vibration analysis in the frequency domain", Ph.D. Thesis, University of Granada, Spain.
- Rotondo, B. and Barbat, A. (2004), "Diseño sismorresistente de edificios: técnicas convencionales y avanzadas", Reverté.
- Rytter, A. (1993), "Vibration based inspection of civil engineering structures", Ph.D. Thesis, Aalborg University, Denmark.
- Symans, M.D., Charney, F.A., Whittaker, A.S., Constantinou, M.C., Kircher, C.A., Johnson, M.W. and McNamara, R.J. (2008), "Energy dissipation systems for seismic applications: Current practice and recent developments", *J. Struct. Eng.*, **134**(1), 3-21.